NOVEL CARBON ADSORBENTS FOR FUEL GAS STORAGE DERIVED FROM LIGNOSULFONATE WASTE

Emmanuelle Alain[1], Brian McEnaney [1], Oleksandr Kozynchenko [2,3], and Vladimir Strelko [2]

[1] Materials Research Centre, Department of Engineering and Applied Science, University of Bath, Bath, BA2 7AY, United Kingdom.

[2] National Academy of Sciences, Institute of Sorption and Problems of Endoecology, Kiev, Ukraine.

[3] MAST Carbon Ltd, Henley Park, Guilford, GU3 2AF, United Kingdom

KEYWORDS   carbon adsorbents, fuel gas, lignosulfonate waste

INTRODUCTION

There has been a resurgence of interest in using adsorbent carbons for fuel gas storage (natural gas and hydrogen). Molecular simulations of adsorption at ambient temperatures of methane (as a model for natural gas) [1] in slit-shaped carbon pores indicate an optimal micropore width for methane storage of ~11 Å. Thus, to optimise the storage capacity requires maximisation of micropore volume, of about this width, and minimisation of mesoporosity, macroporosity and void space between the carbon particles [2]. A storage system for road vehicles powered by natural gas requires a delivered volumetric capacity of ~150 v/v. These requirements have prompted the development of a number of routes for fabrication of highly microporous carbon monoliths with storage capacities that approach or meet the target [e.g., 2-5]. Thus, future work should be aimed towards the development of carbon monoliths by inexpensive and flexible methods. In this paper we report the preparation and characterisation of activated carbon monoliths from lignosulfonate resins derived from waste products in the paper pulp industry.

EXPERIMENTAL

Precursor Materials.   Lignin is a high molecular weight, polyphenolic biopolymer and an important constituent of wood (~30 wt% dry basis). Lignosulfonates are waste products of the paper pulp industry formed by treatment of wood with strong alkali solutions saturated with sulphur dioxide. The lignosulfonate used in this study was received as a sodium salt from the Kondopoga plant in the north of European Russia. Spherical lignosulfonate resins were produced by emulsion, polycondensation reactions with cross-linking reagents; the details of the formulations used for the polymerisations are proprietary.

Carbon Microbeads.   Spherical resin beads, M1, were carbonised in flowing argon by heating to 900 °C to produce carbon beads, M2. Heating in flowing carbon dioxide at 900 °C for different times produced two activated carbons M3 and M4 with 44 and 55 wt% burn-off respectively. A third activated carbon bead sample (59 wt % burn-off), L5, was made in the same way, but starting from a resin produced from a different polymerisation formulation.

Resin and Carbon Discs.   The resin microbeads were pressed into resin discs (4.0 x 0.1 cm), A-1, at 100 °C and 3.2 kN cm^{-2}. Carbon discs, A-3, were prepared from A-1 by carbonisation in CO_2 at 600 °C for 1.5 h. An activated carbon disc, D-4, was prepared by addition of the activation catalyst potassium acetate (2 wt% K$^+$) to resin microbeads prior to pressing into discs. The discs were then carbonised/activated by heating to 600 °C for 1.5 h. The burn-off of the activated carbon discs was estimated as 25-30%. The various routes for the production of carbons from the resin microbeads are summarised in Figure 1.

Characterisation Methods. The general morphology of the bead and disc samples was studied using SEM (JEOL 6310). Samples were spread on a graphite pad and gold sputtered. The packing density of the bead samples and piece (bulk) densities of the disc samples were measured using standard methods. Surface areas and micropore volumes were determined from N_2 adsorption at 77 K (Micromeritics ASAP 2010). Methane adsorption at 298 K and up to 8 bar was measured gravimetrically using a Hiden Intelligent Gravimetric Analyser.

RESULTS AND DISCUSSIONS

Microscopy.   The spherical resin, M1, Figure 2(a), consists mainly of agglomerated spheres with a wide range of diameters (70-800 μm); only the largest microbeads are isolated. The extent of agglomeration in the carbon spheres, M2, and the activated spherical carbon, M3, M4, is much reduced and many more isolated particles are found, Figure 2(b)-(c). There is evidence for preferential attack at former points of contact in the case of the activated carbon

beads and broken particles reveal that some are solid spheres while others have hollow centres (shells). The same observations apply to the L5 sample. A comparison of the resin disc A-1, the carbon disc A-3 and the activated carbon disc D-4, Figure 3, illustrates the volumetric shrinkage (~67%) that occurs upon carbonisation. SEM of the discs, Figure 2 (d), shows that the pressing process leads to agglomeration of the resin microbeads and in some areas of the discs there is a transformation to a continuous structure.

Nitrogen Isotherms.   Adsorption of nitrogen at 77 K on the carbon microbeads M2, Figure 4(a), and the activated carbons M3 and M4 indicate qualitatively that the carbons are microporous. For the activated carbons there is hysteresis at high relative pressures (P/Po >0.8) that is type H1 in the IUPAC classification [6]. This is attributed to condensation in the interstices between the carbon spheres. The isotherm of the carbon material L5, Figure 4(b) shows hysteresis of type H3 that is indicative of a small amount of mesoporosity. This shows that the pore structure of the carbon beads can be controlled to some extent by varying the polymerisation conditions. The nitrogen adsorption isotherms for the carbon discs, A-3 and D-4, at low relative pressure, Figure 4(c), are more rectangular than those for the loose spherical carbons, indicating that they contain narrow micropores. Type H4 hysteresis is seen, indicative of microporosity with a type I isotherm. The gravimetric adsorptive capacities of the carbon discs are clearly less than those of the carbon microbeads, as reflected in the BET surface areas of the carbons, Table 1, and the micropore volumes, V_0, determined using the Dubinin-Astakhov equation.

Methane Adsorption.   Gravimetric isotherms for adsorption of methane at 298 K on activated carbons M4 and L5 and activated carbon disc D-4 are in Figure 5. It is notable that the gravimetric methane uptake by the activated carbon disc D-4 up to ~4 bar is comparable to the uptake by the activated carbon beads M4 and L5. This is in contrast to nitrogen uptake by these carbons, Figure 4.
The maximum pressure attainable in this study is 8 bar, but the practical target storage pressure for methane is 34 bar. We have shown previously [7] that the gravimetric capacity at 34 bar, $n(P)$, can be estimated accurately by extrapolation from the lower pressure data using the Tóth adsorption isotherm equation [8]:

$$n(P) = (\frac{mP}{b+P^t})^{1/t}$$ (1)

where m, b and t are parameters of the equation obtained by curve fitting. Estimates of $n(P)$ at 34 bar and measured values for 1 bar for the activated carbon microbeads M4 and L5 and the activated carbon disc D-4 are given in Table 2. As indicated in Figure 5, the gravimetric capacity, $n(P)$, for the activated carbon discs D-4 at 34 bar is lower than those for the activated carbon spheres M4 and L5, but the reverse is true at 1 bar. This is another indication that the carbon discs have narrower micropores than do the carbon microbeads.

Volumetric Methane Capacities.   The key criterion for evaluating the suitability of activated carbons for natural gas storage is the volumetric capacity expressed as volume of methane at 298 K per volume of activated carbon, including inter-particle voids. Three methane capacities can be taken into account: the adsorbed, the stored and the delivered capacities. *The adsorbed capacity*, V_a, is defined as the excess volume of methane adsorbed in micropores per volume of activated carbon. The adsorption isotherm expressed as gravimetric methane uptake, $n(P)$/mmol g^{-1} vs. P is an excess isotherm which measures the excess methane adsorbed in pores, excluding methane stored in the gas phase. It is given by

$$V_a = 24.465n(P)\rho_a$$ (2)

where ρ_a is the packing density for powders or the bulk (piece) density for monoliths. *The stored capacity*, V_s, is defined as the sum of methane stored in the adsorbed phase, V_a, and in the gas phase, V_g, at pressure, P, (3.4 MPa, 34 bar) where

$$V_g = \frac{PV_t\rho_a}{zP_o} \sim 36V_t\rho_a$$ (3)

and z is the compressibility of methane at P (= 0.93 at 34 MPa and 298 K), P_o is a reference pressure (1 bar) and V_t, the total pore volume, including micropores, mesopores, macropores and inter-particle voids.

$$V_t = (1 - \frac{\rho_a}{\rho_c}) \sim (1 - 0.5\rho_a)$$ (4)

where ρ_c is the skeletal density of solid carbon ($\rho_c \sim 2.0$ g cm^{-3}). There is an uncertainty on whether or not the micropore volume should be included in the calculation of compressed methane gas in pores. If the micropores are fully occupied by adsorbed gas, then they should be

excluded from the calculation. In reality, the stored methane capacity should lie between the two extreme values:

$$V_s = V_a + 36(1 - 0.5\rho_a)$$
$$V_s = V_a + 36(1 - 0.5\rho_a - V_0\rho_a)$$

(5) (a) (b)

The delivered capacity, V_d, is simply the difference between the stored capacity at the storage pressure (3.4MPa, 34 bar) and the stored capacity at the release pressure (0.1 MPa, 1 bar)

$$V_d = V_s(3.4MPa) - V_s(0.1MPa)$$

(6)

Table 2 shows that although the activated carbon beads M4 have the highest gravimetric methane capacity, the activated carbon disc has the highest stored and delivered capacity. Here, the lower gravimetric capacity of the discs is offset by their higher bulk density. By contrast, the delivered volumetric methane capacities of the carbon microbeads are modest due to the high volume fraction of inter-particle voids. The delivered capacities found for the activated carbon discs, D-4, approach the target value of 150 v/v. It is likely that this target can be achieved with further refinement of the microstructure of the carbons. For example the value of V_a (= 36 v/v) found for the discs D-4 at 1 bar is almost twice the values found for the loose activated carbon spheres. This is another reflection of the presence of narrow micropores in the carbon discs. The amount of methane retained in the discs at 1 bar can be reduced if the micropore size distribution can be widened slightly.

CONCLUSIONS

Porous spherical resins of different particle sizes can be produced by emulsion polycondensation of lignosulfonates with cross linking agents. These resin can be converted directly into activated carbon beads or pressed into discs that can be converted into activated carbon monoliths. The delivered volumetric capacities of the loose activated carbons are modest (~81-112 v/v) due to the high volume fraction of inter-particle voids. The delivered capacity of the activated carbon discs approach the target capacity of 150 v/v. The flexibility of the fabrication route for producing carbons from lignosulfonate resins suggests that this target can be reached with further development.

REFERENCES

1. Matranga, K.R., Myers, A.L. and Glandt, E.D., *Chem. Eng. Sci.*,**47** (1992) 1569
2. Chen, X.S., McEnaney, B., Mays, T.J., Alcaniz-Monge, J., Cazorla-Amoros, D. and Linares-Solano, A., *Carbon*, **35** (1997) 1251
3. Quinn, D.F. and MacDonald, J.A., *Carbon*, **30** (1992) 1097
4. Bose, T., Chahine, R. and Arnaud, J.M., *US Patent 4999330* (1991)
5. Manzi, S., Valladares, D., Marchese, J. and Zgrablich, G., *Adsorption. Sci. Tech.*, **15** (1997) 301
6. Gregg, S.J. and Sing, K.S.W., *in Adsorption, Surface Area and Porosity*, London, Academic Press (1982)
7. Alain, E., McEnaney, B., Mays, T.J., Strelko, V. and Kozynchencko, O., *Extended Abstracts 'Carbon'99'*, American Carbon Society, Charleston, SC, USA, (1999) 784
8. Valenzuela, D.P. and Myers, A.L., *in Adsorption equilibrium data handbook*, Prentice Hall, Englewood Cliffs, (1989) 8

Table 1. Particle bulk densities, ρ_a, BET surface areas, S_{BET}, and D-A micropore volumes, V_0 for activated lignosulfonate carbons.

Material	ρ_a /(g cm^{-3})	S_{BET}/(m^{2}g^{-1})	V_0/cm^3 g^{-1})
Spherical activated carbons, M3	0.37	1202	0.64
Spherical activated carbons, M4	0.33	1610	0.92
Spherical activated carbons, L5	0.47	1235	0.58
Activated carbon discs, A-3	1.26	335	0.17
Activated carbon discs, D-4	0.95	676	0.33

Table 2. Methane capacities at 298 K for activated lignosulfonate carbon beads and discs.

Material	$n(P)$/(mmol g^{-1}) 34 &1bar [b]	V_a 34 &1 bar [b]	V_s 34 bar [c]	V_d [c]
Spherical activated carbons M4 (1) [a]	9.5 & 1.4	77 & 11	96~107	85~96
Spherical activated carbons M4 (2) [a]	9.1 & 1.4	73 & 11	92~103	81~92
Spherical activated carbons L5 (1) [a]	8.6 & 1.3	99 & 15	117~126	102~111
Spherical activated carbons L5 (2) [a]	8.7 & 1.3	100 & 15	118~127	103~112
Activated carbon discs D-4	6.5 & 1.6	152 & 36	159~170	123~134

a. Duplicate samples.
b. Values at 34 bar estimated using the Tóth equation, measured values at 1 bar.
c. Higher and lower values calculated using Equation 5 (a) and 5 (b) resp.
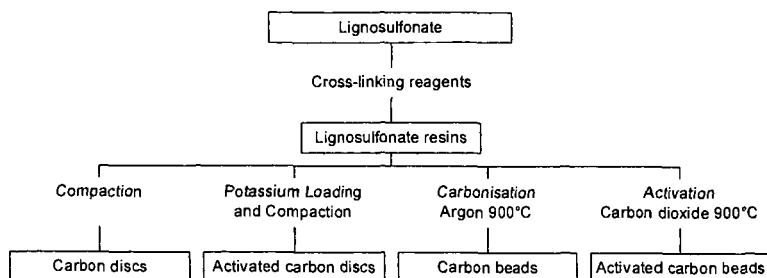

Figure 1. Flow diagram for production of the carbons derived from lignosulfonate resins.
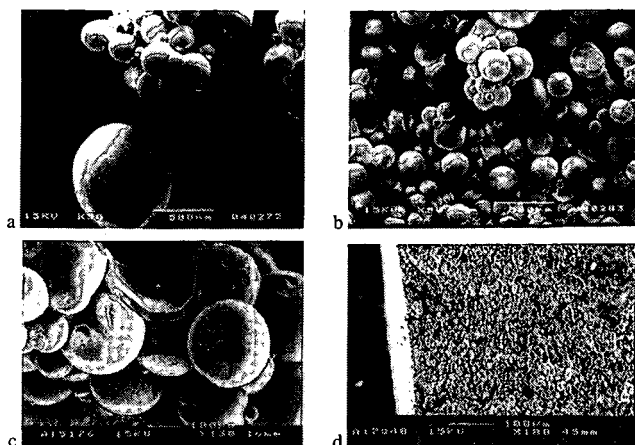
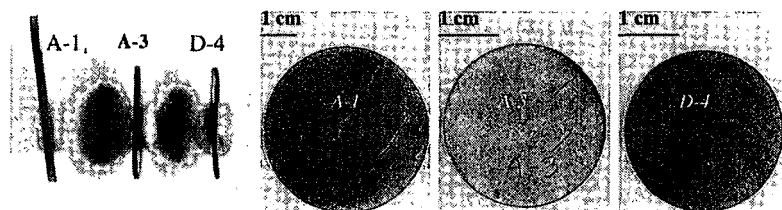Figure 2 (a)-(d). SEM micrographs of the carbons

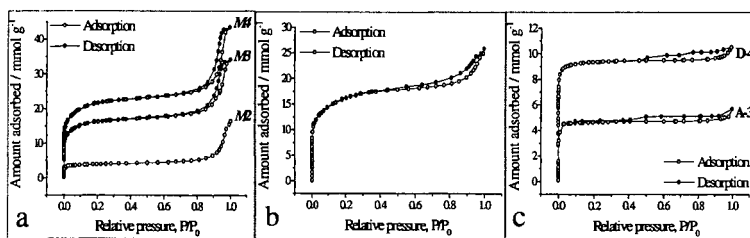
Figure 3. Optical macrographs of the discs

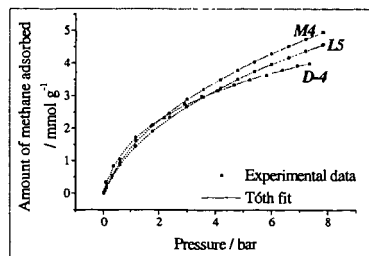Figure 4. Nitrogen adsorption isotherms (a) M2-M4; (b) L5; (c) A-3, D-4.

Figure 5. Measured methane isotherms at 298K and their Tóth fits.

MECHANISMS OF MERCURY CAPTURE AND BREAKTHROUGH

ON ACTIVATED CARBON SORBENTS

Edwin S. Olson, Grant E. Dunham, Ramesh K. Sharma, Stanley J. Miller

Energy & Environmental Research Center, University of North Dakota

Grand Forks, ND 58202

KEYWORDS: mercury sorbent, activated carbon

ABSTRACT

An extensive series of studies was performed at the Energy & Environmental Research Center with mercury (Hg^0) sorbents in a thin bed using combinations of various flue gas constituents. This work determined that all the sorbents exhibited breakthrough in about 1 hour in the full flue gas mixture, and the mercury emitted after breakthrough is an oxidized mercury species. Trapping of the oxidized species and identification by mass spectrometry demonstrated that both carbon and metal oxide sorbents release the relatively volatile mercuric nitrate hydrate when both NO_2, SO_2, and water vapor are present in the gas phase. Further investigations of treated sorbents allow us to determine the role of oxidation and basic sites on the sorbent in the capture of mercury in NO_2 and SO_2 streams.

INTRODUCTION

There is currently intense interest in discovering effective sorbents for the control of mercury emissions in flue gas from coal-burning utilities. Extensive factorial evaluations of powdered sorbents were conducted at the Energy & Environmental Research Center in a bench-scale system consisting of a thin fixed-bed reactor in gas streams containing 15 $\mu g/m^3$ of elemental mercury (Hg^0) in various flue gas components and simulated mixtures (1). One of the effective sorbents tested was the commercial powdered carbon sorbent Norit FGD, which is a lignite-derived activated carbon (LAC), and this carbon was selected for more extensive testing to determine the critical factors involved in mercury capture. The previous results showed that in an atmosphere containing an acid gas such as HCl or NO_2, effective capture of Hg^0 from the gas phase occurred on activated carbon sorbents at temperatures of 100° to 150°C. Without either of these acid components in the gas stream, the carbon sorbents are ineffective, and immediate breakthrough occurred.

In tests conducted in the simulated flue gas containing NO_2 but not SO_2, very little breakthrough was observed over an extended time period, indicating that the bound mercury form is quite stable. The capture is attributed to oxidation of the Hg^0 and concomitant reduction of NO_2 with formation of a low-volatile oxidized mercury species that remains bonded to the sorbent. Reactions of Hg^0 with NO and NO_2 in a glass container were previously reported to form mercuric oxide and mercuric nitrate/nitrite mixtures (2–3).

When SO_2 was added to the gas mixture containing the NO_2, the mercury sorption rate was initially high (98% of inlet Hg^0 was sorbed); however, breakthrough occurred after 1 hr at the 225°F conditions. The breakthrough curve was relatively steep, increasing to 100% or greater emission after about 2 hr. Not only is mercury no longer sorbed, but mercury sorbed earlier in the experiment is released. Thus there is a significant interaction effect for SO_2 and NO_2 on the sorbent breakthrough time.

The mercury that is emitted from the sorbent after breakthrough is entirely an oxidized mercury species. In reactions conducted with NO_2 and SO_2 and no HCl, this volatile oxidized mercury product was identified as mercuric nitrate hydrate (4). The formation of the mercuric nitrate hydrate from reactions of Hg^0 and NO_2 was not reported in the early literature. It is surprising that SO_2 appears to facilitate the release of the volatile mercuric nitrate hydrate from the sorbent surface. The early breakthrough effect was observed for a number of different sorbents in the flue gas stream containing both NO_2 and SO_2. This appears to be the controlling element in sorption capacity for mercury in flue gas. Since the effect lowers the capacity and defeats the effectiveness of all the sorbents tested, is important to understand the nature of this interaction and to determine the carbon-related factors that determine the reactivity of the carbon sorbent and its ability to stabilize the oxidized mercury against release as volatile salts. An adequate model for the sorption and breakthrough mechanism is needed to design effective sorbents for mercury control in flue gas.

The work reported in this paper concerns the carbon-related factors that determine the breakthrough behavior in the NO_2–SO_2 stream. Two of these factors are the role of inorganic matter

present in the carbon and the role of catalytic surfaces on the carbon. The hypotheses to be tested are that basic inorganic constituents of the carbons are able to bind mercury by forming relatively stable basic mercury salts and that these basic sites are exhausted by continued exposure to SO_2. Release of Hg(II) would occur at breakthrough when the basic binding sites are exhausted.

The much higher reactivities observed previously for mercury sorption in air with catalytic carbons compared to noncatalytic carbons lead to the hypothesis that sorption in NO_2 can also occur at different types of sites and involve formation of different intermediate species. Comparison of the breakthrough curves for the two types of carbons should elucidate these mechanisms.

RESULTS

To determine whether inorganic sites on the activated carbons are an important factor in mercury sorption in flue gas, carbons with various levels of inorganic constituents were tested. The Norit FGD sorbent that is active for mercury capture in flue gas streams is a finely powdered unwashed LAC. This means that it has a relatively high ash or inorganic content. This carbon is produced from a lignite with high calcium content, so part of the calcium is present in the carbon as the oxide and gives the surface a basic nature. The granular form of the LAC carbon is also available commercially (Norit GAC 1240), but in contrast to the powdered FGD sorbent, the granular lignite-derived carbon is acid-washed to remove some of the inorganic material in the carbon. In previous studies in air, neither the GAC 1240 or the powdered FGD carbon were effective for mercury capture. A ground sample of the GAC 1240 had not been tested for mercury capture in flue gas streams, so it was important to determine if the lower amounts of inorganic constituents on the washed carbon result in shorter breakthrough times owing to a lower capacity for retaining oxidized mercury.

The sorption test performed with the ground sample of commercial acid-washed GAC 1240 in the synthetic flue gas stream showed that the sorption activity was excellent at the start, and breakthrough was not observed for 1.7 hr, compared to 1 hr for LAC. The extended breakthrough results from this experiment are, therefore, not consistent with the concept that basic inorganic material on the surface is required for effective mercury sorption.

To further test the hypothesis that basic surfaces are important for effective mercury control, the Norit FGD carbon was washed with dilute nitric acid to remove basic calcium, iron, and sodium oxides. The demineralized carbon was tested in the synthetic flue gas stream, and results were compared with the initial FGD carbon under the same conditions of temperature, flow rate, and gas composition. The results with the washed FGD (Run 945) were identical to those from the original FGD carbon. Breakthrough occurred at 1 hr and later sampling showed that most of the Hg in the effluent from the sorbent bed was oxidized. Thus removal of basic sites by washing the sorbent with nitric acid did not result in less effective sorption.

Catalytic carbons were previously shown to exhibit very high mercury sorption activities in air streams (5). Not only were high initial kinetics for sorption observed, but the activities decreased only very gradually over several days of testing. But is this higher sorption activity for the catalytic carbons in air also observed in the simulated flue gas system?

The results of testing a catalytic carbon in the bench-scale simulated flue gas showed that the sorption curve is very similar to that of the LAC sorbent and that breakthrough occurred at the same 1-hr point in the experiment as observed for the LAC. Only oxidized mercury is observed in the emission after breakthrough. Thus the catalytic carbon is subject to the same NO_2–SO_2 interaction as the LAC.
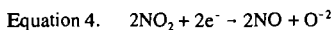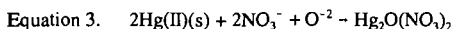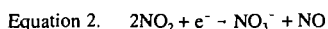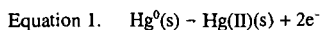
DISCUSSION

The results with washed carbons do not support the hypothesis that basic inorganic residues in the carbon are involved in binding oxidized mercury, since shorter breakthrough times resulting from failure to bind Hg(II) at basic inorganic sites were not observed. The better capacity exhibited by the ground sample of GAC 1240 may be explained by the cleaning effect of the acid in removing basic salts that are plugging the carbon pores and, therefore, improve internal mass transport. Secondly, the removal of inorganic material may expose more carbon surface and, therefore, more oxidation sites, which may overcome the negative effect expected for removal of the basic sites. Thirdly, there may be other binding sites on the carbon structure that would have been exposed by the removal of the basic inorganic sites. It is possible that some residue from the wash solution somehow improved the capacity of the GAC 1240.

The experiments do not, however, rule out the involvement of inorganic matter since it could be argued that the washing procedure removed mineral matter only from the mesopores. This would improve the internal mass transfer, but still leave some basic sites available on the micropore surface for converting the Hg(II) to nonvolatile basic salts. Thus the failure of the experiments to demonstrate decreased capacity does not reject the basic inorganic residue hypothesis, but other experiments must be conducted to determine which effects are occurring. The significantly better performance (longer breakthrough time) of the GAC 1240 cannot be adequately explained until further information on these factors is available.

The air oxidation mechanisms of catalytic carbons appear to be quite different than those of noncatalytic carbons. Reactions with NO_2 could also involve different mechanisms and form different intermediate species in the two types of carbons. However, this work shows that the oxidation mechanisms using NO_2 as the primary oxidant (electron sink) may be the same in the catalytic and noncatalytic carbons. The similarity in breakthrough times for the two types of carbons appears to reject the hypothesis that intermediate species are different for the two carbons.

A simple model for the sorption reaction is that the adsorbed $Hg^0(s)$ is rapidly oxidized at an oxidation site on the carbon surface to a bound Hg (II) species utilizing electrons from the NO_2 (Equations 1-2). This reaction is likely to occur readily on any kind of carbon surface as well as other surfaces. In the absence of SO_2, the major species formed would be mercuric oxide or a basic mercuric nitrate/oxide (Equation 3), which is stable at 150°C, even in the stream containing NO_2. Oxide could be present on the sorbent surface initially (such as CaO) or could be produced from NO_2 as shown in Equation 4. The stable basic mercury salts collect in sites adjacent to the oxidation site, and the activated carbon is able to retain relatively large amounts of these forms. Thus this model is consistent with the behavior of both catalytic and LAC carbons.
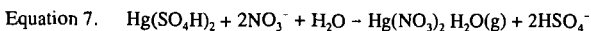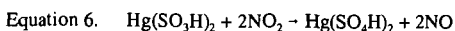
Equation 1. $Hg^0(s) \rightarrow Hg(II)(s) + 2e^-$

Equation 2. $2NO_2 + e^- \rightarrow NO_3^- + NO$

Equation 3. $2Hg(II)(s) + 2NO_3^- + O^{-2} \rightarrow Hg_2O(NO_3)_2$

Equation 4. $2NO_2 + 2e^- \rightarrow 2NO + O^{-2}$

The role of SO_2 in the breakthrough mechanism is more difficult to understand. Since the oxidation of Hg^0 is still 100% at breakthrough, it is unlikely that SO_2 is inhibiting the Oxidation Reaction 1 and, therefore, the oxidation sites. It must also not inhibit Reactions 2 and 4, since SO_2 can not provide the electron sink for Hg^0 oxidation and is not normally reduced on a carbon surface. Therefore, SO_2 must be involved in the reactions leading to mercury stabilization on the sorbent or to bonding of the Hg (II) species formed in or subsequent to the oxidation.

Thus a direct involvement involving binding of SO_2 to an intermediate bound Hg(II) species seems more likely. In the presence of adsorbed SO_2, the Hg(II) may react to initially form mercuric sulfite or hydrosulfite (Equation 5). These species have Hg–S bonds and are expected to be nonvolatile. This nonvolatile species also collects in sites adjacent to the oxidation site. This form is consistent with the XAFS study (6) that concluded that mercury is bound by either sulfur or chloride on the sorbent.

Equation 5. $Hg(II)(s) + 2HSO_3^- \rightarrow Hg(SO_3H)_2$
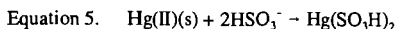
Over time (1 hr), this form could be oxidized to mercury sulfate or bisulfate which results in forming Hg–O bonds (Equation 6). These bonds will be more labile, and interconversion to the volatile mercuric nitrate hydrate occurs (Equation 7). Since no Hg^0 is emitted, the oxidation sites must still be functioning at breakthrough, only the bonding sites are becoming ineffective. This model is inadequate, however, because it predicts a gradual breakthrough from the start rather than the sudden one that is observed after 1 hr. Thus there seems to be other missing structural or reactivity factors that have not yet been considered.

Equation 6. $Hg(SO_3H)_2 + 2NO_2 \rightarrow Hg(SO_4H)_2 + 2NO$

Equation 7. $Hg(SO_4H)_2 + 2NO_3^- + H_2O \rightarrow Hg(NO_3)_2 \cdot H_2O(g) + 2HSO_4^-$

The original hypothesis was that the LAC uses inorganic CaO sites to aid in the conversion of the oxidized Hg(II) (Equation 4) to the basic mercuric nitrate oxide that is not volatile and these sites are eventually converted to $CaSO_3$ or $CaSO_4$ that are inactive for stabilization. But this is not likely since removal of CaO did not shorten breakthrough.

The alternative model we now wish to consider is that SO_2 reacts with oxide at the carbon surface. By complexing these basic sites, this reaction may interfere with the formation of the stable basic mercuric oxide salt, as well as use up SO_2 that would bind directly to the mercury. Further experiments are needed to test this model.

ACKNOWLEDGMENTS

REFERENCES

1. Miller, S.J.; Dunham, G.E.; Olson, E.S. "Mercury Sorbent Development for Coal-Fired Boilers," *In* Proceedings of the Air Quality Conference, McLean, VA, Dec. 1, 1998.
2. Pierce, W.C.; Noyes, W.A. *J. Amer. Chem. Soc.* **1928**, *50*, 2179.
3. Freeman, E.S.; Gordon, S. *J. Amer. Chem. Soc.* **1956**, *78*, 1813.
4. Olson, E.S.; Sharma, R.K.; Miller, S.J. Dunham, G.E. Mercury in the Environment, Proceedings of a Specialty Conference, VIP-91, Air & Waste Manag. Assoc., Minneapolis, MN, Sept 15, 1999, p 121.
5. Olson, E.S.; Sharma, R.K.; Miller, S.J.; Dunham, G.E. *Preprints: Div. Fuel Chem., Am. Chem. Soc.* **1998**, *43*, 867.
6. Huggins, F.E.; Huffman, G.P.; Dunham, G.E.; Senior, C.L. *Energy & Fuels* **1999**, *13*, 114.

ACTIVATED CARBONS IN EXTRACORPOREAL METHODS
OF MEDICAL TREATMENT - TIME TO REACTIVATE THE IDEA?

Sergey Mikhalovsky

School of Pharmacy and Biomolecular Sciences

University of Brighton

Brighton BN2 4GJ, U.K.

KEYWORDS: Haemoperfusion, extracorporeal therapy, polymer-pyrolysed activated carbon

INTRODUCTION

The term "extracorporeal therapy" means a medical treatment utilising an extracorporeal circuit. Blood, plasma or another body fluid is passed through the extracorporeal purification device, where the toxic substances are separated and the purified fluid returns to the body. A range of extracorporeal therapies are available at present, based on physical (dialysis or filtration) or physicochemical (adsorption) mechanisms (Table 1).

Table 1. Physical and physico-chemical principles of extracorporeal therapy.

Method	Principle
Haemodialysis (HD)	Diffusion and convective transport through a semipermeable membrane, osmosis
Haemofiltration (HF)	Ultrafiltration and convective transport of solutes across a semipermeable membrane or filter
Combined HD/HF, or haemodiafiltration	Diffusion, ultrafiltration and convective transport
Apheresis and plasmapheresis	Membrane or centrifuge separation of blood into cells and plasma and further plasma fractionation using various methods
Haemoadsorption, or haemoperfusion (HP)	Physical adsorption, ion exchange or chemisorption

The concept of extracorporeal therapy (dialysis) can be traced back as early as 1913 [1], and the use of activated carbons in medicine for detoxification has been known since ancient Egypt and Greece [2], but real progress in the development and clinical applications of extracorporeal methods was made in 1960s-1980s. During these three decades commercial devices for extracorporeal treatment became available. Although extracorporeal adsorption was introduced along with dialysis and filtration, currently its use is limited to acute poisoning with low molecular drugs, whereas dialysis and filtration are widely used for the treatment of acute poisoning, acute and chronic organ failure and in various life support systems [3-6]. It is shown in this paper that recent progress in carbon science makes adsorption over activated carbons competitive to other extracorporeal methods. Current status, problems and prospects of extracorporeal adsorption therapy are discussed.

BIOCOMPATIBILITY OF ACTIVATED CARBONS

The first clinical use of charcoal in a HP device was reported by Yatsidis [7]. Haemoperfusion was carried out on a column of 200 g charcoal at a flow rate of 150-300 ml/min for 30-90 min. The results of the treatment of patients with terminal chronic renal failure were encouraging, and the charcoal column efficiently removed creatinine, uric acid and other uraemic metabolites. It was estimated that a 60-min HP was as efficient as a 4 to 6-hr HD. Blood perfusion over activated carbon was also successfully used for treatment of acute poisoning. However, this procedure induced hypotension, reduction in glucose, calcium and potassium concentration and damaged blood cells [8,9]. The most severe problem was the release of fine particles from the carbon granules causing microemboli. Despite thorough washing, microparticles of 5-35 μm size were persistently detected in the blood samples and washing solutions at the outlet of the carbon column. Use of plasma perfusion followed by its filtration to remove fine particles, instead of blood perfusion was suggested [10].

The problem of fine particle release from activated carbon granules was solved by coating them with a semipermeable membrane [9,11]. The most common commercially available activated

carbon haemoperfusion column 'Adsorba' is manufactured by Gambro, Sweden/Germany. In the 'Adsorba' column, Norit RXS extruded peat charcoal is coated with a 3-5 µm thick cellulose membrane. Coating carbon granules makes them more biocompatible but it also dramatically affects performance of a haemoperfusion column reducing the rate of diffusion to the carbon surface and efficiency of haemoperfusion. Adsorption of high molecular weight solutes is particularly affected. A thick membrane virtually cuts off HMW molecules and significantly reduces adsorption of "middle molecules" with molecular mass between 300 and 15,000 [12]. Removal of 'middle molecules' is essential as they play an important role in the development of many pathological conditions.
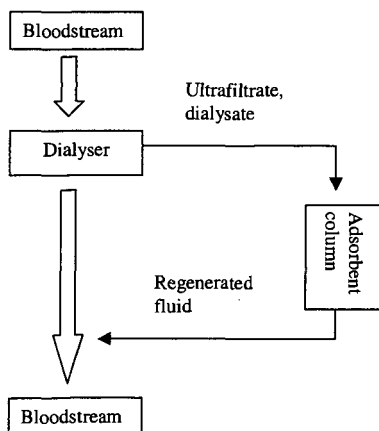
Use of coated adsorbents instead of uncoated dramatically reduces efficiency of haemoperfusion both in terms of adsorption capacity and rate of adsorption. Not surprisingly, information about the ability of coated activated carbons to remove even low molecular uraemic toxins is controversial [13]. As a result, HP has been limited in use to only acute poisoning with certain low molecular toxins [14].

UNCOATED ACTIVATED CARBONS FOR EXTRACORPOREAL THERAPY

The growing economic pressure on medical care provides a strong incentive for further development of adsorption therapy [15]. Patients in need of chronic extracorporeal treatment are usually of advanced age, and their number is rapidly increasing. For example, by the middle of this century the number of 75+ aged people will have doubled and the population over age 90 will have more than tripled in the U.K. [16]. This will result in a heavy burden on NHS. A similar situation is happening in other developed countries. Current expenditures on the treatment of chronic renal, liver and multiorgan failure – life threatening conditions in which HD and HF are widely used, far exceed the health care funding of all but a few nations [15]. Unless a cost-effective solution is found, this situation can only worsen.

An adsorption column could be used in-line with HD or HF to reduce the cost of treatment and achieve higher efficiency. Current dialysis membranes remove about 10-40% of middle molecular weight toxins. It has been found that up to 100% of this amount is removed by adsorption to the membrane surface which is about 1-2 m^2 g^{-1} [17]. The surface area of an activated carbon is much higher. Thus, the capacity for removal of middle molecular weight toxins by adsorption far exceeds that of dialysis.

Use of dialysis or filtration technique inevitably results in a loss of large volume of water along with dissolved useful metabolites and nutrients. To compensate for such a loss, an isotonic and sterile replacement fluid is provided. In the treatment of intensive care patients who develop acute renal failure more than 50% of the total cost of HD or HF is associated with the purchase of replacement fluid [18]. In-line adsorption would increase efficiency of the extracorporeal procedure and reduce the loss of liquid by its recycling (Scheme).

Bloodstream

Ultrafiltrate, dialysate

Dialyser

Adsorbent column

Regenerated fluid

Bloodstream

Scheme.

In-line use of adsorbent column with HD or HF.

In this circuit the adsorbent does not come into contact with blood directly and the biocompatibility problem is reduced significantly.

A recently developed "BioLogic-DT" system combines haemodialysis and adsorption in one unit, utilising a carbon powder suspension to accelerate removal of toxins from blood [19]. In this system blood passes through a dialysis cellulose membrane package surrounded by a

suspension of fine particles of an activated carbon and a cation exchanger. The adsorbent and the blood are separated by a membrane. Removal of LMW toxins is accelerated by the adsorption mechanism that increases the concentration gradient across the dialysis membrane.

A similar approach has been suggested in a **M**icrospheres **B**ased **D**etoxification system (MDS) [20]. In this case blood is separated from plasma in the first circuit, and an adsorbent suspension is used in the secondary circuit for plasma purification. Although cellulose microbeads were used in the first instance, the system allows for the use of any other microparticles including activated carbon.

A specific problem with in-line carbon adsorption is related to its low adsorption capacity towards urea. Urea is one of the substances-markers of renal failure and it is efficiently removed from blood by dialysis. To tackle this problem, the ultrafiltrate regenerated by adsorption is infused into the additional diffusive dialyser that removes urea and then it is returned to the bloodstream. [21].

UNCOATED ACTIVATED CARBONS FOR DIRECT HAEMOPERFUSION

A much more challenging problem is synthesis of uncoated activated carbons that are as haemocompatible as coated adsorbents. Neither the exact nature of bio/haemocompatibility, nor the mechanism of 'blood-foreign surface' interactions are fully understood [22]. Despite this uncertainty, there is a general agreement that a haemocompatible material should meet the following criteria: (i) absence of thrombogenic, toxic, allergic or inflammatory reactions; (ii) no damage of blood cells or adjacent tissue; (iii) no undesirable changes in the blood composition; (iv) no immunological reaction; (v) no carcinogenic effect [23].

Carbon surface is considered to be rather biocompatible and some artificial organs are made from carbon materials. Such materials, however, have low surface area. The problem could be solved using activated carbons produced from synthetic polymers [24,25].

Using synthetic polymers as the precursor material eliminates any uncontrolled impurities. Coated activated carbons used for HP are made from natural raw materials. They have never been designed specifically for medical applications. In fact, they were technical grade carbons taken 'off the shelf' and used after a very simple pretreatment with hydrochloric acid and/or deionised water. Further pre-treatment such as electrolyte balancing is necessary to adjust the ionic composition of the carbon surface to the mineral composition of the blood. The fact that carbon surface contains a variety of functional groups having ion exchange properties, has been frequently ignored resulting in significant changes of pH and ion composition of the blood brought in contact with activated carbon.

It has been shown that two conflicting properties - large surface area and high mechanical strength – could be combined in polymer pyrolysed activated carbons. Thus a simple washing procedure removes microparticles from carbon granules eliminating the major concern about carbon biocompatibility.

Pore size distribution of activated carbons can be controlled by using porous polymeric precursors. In addition to micropores, polymer pyrolysed activated carbons have a unique mesoporous structure within 10-100 nm range which is predetermined by the pore size of the precursor.

It has been shown that mesoporous carbons possess high adsorption capacity towards middle and large protein molecules [26]. This is of particular importance for treatment of autoimmune diseases when removal of HMW immune complexes is necessary.
Activated carbons are considered to be non-specific adsorbents. Whilst high adsorption selectivity is desirable, nonspecific adsorption is also an advantage especially in the treatment of disorders with unknown etiology.

Despite chemically inertness of carbon, generation of chemically reactive functional groups such as -COOH, -NH$_2$ on its surface allows the use of carbon matrix for covalent binding of bioligands [27]. Carbon surface has been activated by oxidation and molecular bioligands have been attached covalently to the carboxylic functional groups via water soluble carbodiimide technique.

Carbon based bioselective adsorbents such as immunoadsorbents could potentially combine the selectivity of a bioligand action and the nonspecific adsorptive capacity of the carbon matrix.
The use of bioselective adsorbents for direct hemoperfusion would eliminate an expensive plasma separation stage.

CONCLUSIONS

The use of adsorbents for regeneration and recycling of dialysate or ultrafiltrate would decrease the volume of extracorporeal devices and relacement fluid, thus significantly reducing operational costs. Direct haemoperfusion over uncoated haemocompatible activated carbon offers more efficient, rapid and cost-effective means of medical treatment as in comparison with other extracorporeal techniques. Research in this area, almost abandoned in the 1980s, is becoming active again and very intensive development of adsorption methods should be expected.

ACKNOWLEDGMENTS

REFERENCES

1. Abel J.J., Rowntree L.G., and Turner B.B., Trans. Assoc. Am. Physns, 1913, **28**, 51.

2. Denti E., and Walker J.M., Activated carbon: Properties, selection, and evaluation, in Giordano, C. (Ed.), Sorbents and Their Clinical Applications, Academic Press, New York, NY, 1980, pp. 101-116.

3. Malchesky, P.S., Artif. Organs, 1994, **18**, 342.

4. Dunea, G., Dialysis versus hemoperfusion in uremia, in Giordano, C. (Ed), Sorbents and Their Clinical Applications, Academic Press, New York, NY, 1980, pp. 375-385.

5. Miller, R., Kingswood, C., Bullen, C., and Cohen, S., Brit. J. Hospital Med., 1990, **43**, 354.

6. Lopukhin, Yu.M., and Molodenkov, M.N., Hemosorption, C V Mosby, St Louis, 1979.

7. Yatzidis, H., Proc. Eur. Dial. Transpl. Assoc., 1964, **1**, 83.

8. Rosenbaum, J.L., Poisonings, in Giordano, C. (Ed.), Sorbents and Their Clinical Applications, Academic Press, New York, NY, 1980, pp. 451-467.

9. Andrade, J.D., Van Wagenen, R., Chen, C., Ghavamian, M., Volder, J., Kirkham, R., and Kolff, W.J., Trans. Am. Soc. Artif. Int. Organs, 1972, **18**, 473.

10. Hagstam, K.E., Larsson, L.E., and Thysell, H., Acta Med. Scand., 1966, **180**, 593.

11. Chang, T.M.S, Trans. Am. Soc. Artif. Int. Organs, 1966, **12**, 13.

12. Vanholder, R., De Smet, R., Vogeleere, P., and Ringoir, S., Artif. Organs, 1995, **19**, 1120.

13. Giordano, C., Esposito, R, Cirillo, D., Betuel, H., Fredel, A., Pluvio, M., Mazzola, G., Longhi, R., and Manzo, M. International J Artif Organs, 1984, **7**, 177.

14. Webb, D., British J Hospital Medicine, 1993, **49**, 493.

15. Friedman, E.A., Artif. Organs, 1992, **16**, 90.

16. Fit for the Future: The Prevention of Dependency in Later Life, Report of the Continuing Care Conference, H. Prophet, ed., June 1998.

17. Swinford, R.D., Baid, S., and Pascual, M., Amer. J. Kidney Diseaases, 1997, **30**, Suppl. 4, S32.

18. Forni,L.G., and Hilton, P.J., Current Concepts, 1997, **336**, 1303.

19. Ash, S.R., Artif. Organs, 1994, **18**, 355.

20. Weber, C., Rajnoch, C., Loth, F., Schima, H., and Falkenhagen, D., Int. J. Artif. Organs, 1994, **17**, 595.

21. deFrancisco, A.L.M., Botella, J., Escallada,R., Hernandez, J., Malo, A.M., Garcia, R.P., Tomero, J.A.S., and Sanz, C., Nephrol., Dial., Transplant., 1997, **12**, 528.

22. Colton, C.K., Ward, R.A., and Shaldon, S., Nephrol., Dial., Transplant., 1994, **9** (Suppl. 2), 11.

23. Klinkmann, H., The role of biomaterials in the application of artificial organs, in Paul J P, Gaylor J D S, Courtney J M, Gilchrist T (Eds), Biomaterials in Artificial Organs, Macmillan Press, London, 1984, pp. 1-8.

24. Strelko, V.V., Korovin, Yu.F., Nikolaev, V.G., Kartel, N.T., and Adamenko, N.P., Uncoated carbon sorbent SCN for direct hemoperfusion, in Piskin E, Chang T M S (Eds), Hemoperfusion and Artificial Organs, Artificial Organs Society, Ankara, Turkey, 1982, pp. 144-146.

25. Lahaye, J., Nanse, G., Bagreev, A., Strelko, V., Carbon, 1999, **37**, 585.

26. Scorgie,K.A., Mikhalovsky, S., Davies, J.G., Olliff, C., Lloyd, A., Phillips, G.J., Street, M., and Kingswood, C., Carbon'99. 24th Biennial Conference on Carbon. Amer. Carbon Soc., Charleston, SC, USA. Extended Abstracts, Vol. 1, pp. 150-151.

27. Mikhalovsky, S.V., Strelko, V.V., Alekseyeva, T.A., and Komissarenko, S.V., Biomat., Art. Cells, Art. Org., 1990, **18**, 671.

UNDERLYING MECHANISM OF DR EQUATION FOR ADSORPTION IN ACTIVATED CARBON

D. D. Do* and C. Nguyen
Department of Chemical Engineering
University of Queensland
St. Lucia, Queensland 4072
Australia

ABSTRACT: The Dubinin-Radushkevich (DR) equation is widely used for adsorption in microporous carbonaceous materials. This equation only yields a macroscopic behaviour of loading for a given pressure. In this paper, we apply our theory (Langmuir, **15**, 3608, 1999) to explain the microscopic adsorption behaviour behind the DR equation.

INTRODUCTION

The Dubinin-Radushkevich (DR) equation is used to describe adsorption of sub-critical fluids in microporous solids such as activated carbon. The DR equation has the form

$$W/W_o = \exp\left[-(A/E)^2\right], \quad A = RT\ln(P/P_0)$$

This equation provides the macroscopic information of the fraction of the total micropore volume occupied by the adsorbate molecules. It does not give any picture on how adsorption behaves microscopically, that is which micropores are filled and which are partially filled as it is well known that activated carbon has a rather broad pore size distribution. This information of microscopic distribution of adsorbed molecules is important in the study of mobility of adsorbed molecules. Here we apply a new method (Nguyen and Do, 1999) to describe the adsorption process in microporous carbonaceous materials with a pore size distribution. It is a structure based method, where enhancement of adsorption is allowed for due to the proximity of the pore walls. We will use this technique to investigate the adsorption in carbon micropores in an attempt to shed some light to the working mechanism of the DR equation.

THEORY

In our approach (Nguyen and Do, 1999) we adopt a common mechanism for the adsorption process occurring in carbonaceous pores as a sequence of surface layering followed by pore filling, irrespective of their sizes. The principal feature of this theory is the allowance for the enhancement in adsorption induced by the overlapping of the potential fields of opposite pore walls. This enhancement not only affects the adsorbed phase, but also the gas phase molecules occluded within the pore. The pressure exerted by these occluded molecules is calculated from:

$$p_p(r) = p\exp(-E_{av}/RT)$$

with E_{av} the average potential energy of the occluded molecules. These occluded molecules will provide source to build up adsorbed layers on the pore walls, following a mechanism akin to BET, but in this theory we take that these layers are enhanced due to the potential energy of interaction with the pore walls. The BET constant in a pore is calculated in terms of the BET constant of a corresponding flat surface as:

$$C_p(r) = C_s \exp\left[(Q_p(r) - Q_s)/RT\right]$$

where $Q_p(r)$ and Q_s are heats of adsorptions in pore and a flat surface, respectively. Adsorption in pores can be pictured as a process whereby gas phase molecules are drawn into the pore interior. Once inside, they are further pressed against each other as a result of the overlapping potential fields. If the pore pressure is beyond the corresponding vapor pressure, the adsorbed phase turns into liquid (albeit compressed liquid). It is, therefore, understood that in some narrow pores, due to the very large enhanced pressures, the adsorbed phase exists as liquid even at very low bulk pressures. This liquid filling process progresses to pores larger in size as the bulk pressure increases. This is essentially the micropore filling process described in the Dubinin theory (1960). In larger pores, adsorption occurs as a surface layering process, and this layer will grow until the following condition is satisfied:

$$r - t - \sigma_{ss}/2 = \gamma v_M / \left[RT\ln(P_0/P_p)\right]$$

when the complete pore filling will occur. Here r is the half width, γ is the surface tension and v_M is the liquid molar volume. The statistical thickness "t" is calculated from:

$$t(r) = t_m \frac{x_p(r)C_p(r)}{\left(1 - x_p(r)\right)\left(1 - x(r) + x_p(r)C_p(r)\right)}; \qquad x_p(r) = \frac{P_p(r)}{P_0}$$

RESULTS & DISCUSSION

The fractional loading in the DR equation defined as $\theta = W/W_o$ accounts for adsorption in micropores only. This means that the contribution of larger pores on the uptake must be removed before they can be used with the DR equation. Furthermore, the DR equation provides only the macroscopic information. For example, when the change in the free energy, A, is equal to the characteristic energy of the system, the fractional loading is 0.37, meaning 37% of the micropore volume is occupied by the adsorbate molecules. Our approach models adsorption as a process occurring in all pores simultaneously, with the amount adsorbed in a pore dependent on the pore size. At a given pressure small micropores are completely filled, while larger micropores have a layer of adsorbate molecules. Knowing the volume of each pore, the overall fractional loading is calculated from:

$$\theta = \sum_j \theta_j W_j / \sum_j W_j$$

where θ_j is the pore fractional loading, and is equal to 1 for filled pores and equal to $t_j/(r_j - \sigma_{ss}/2)$ for pores having layers of adsorbate. This overall fractional loading is then compared with that calculated from the DR equation.

We illustrate this theory with nitrogen adsorption data at 77 K on an ACF sample. This ACF has a micropore volume of 0.24 cc/g, and a mean micropore half width of 0.66 nm. Fitting the DR equation with the data yields the characteristic energy of 6.9 kJ/mol. The distribution of pores calculated by our method is shown in Table 1 (columns 1 and 2) where we show 24 representative pores with their corresponding pore volumes. Using our theory we calculated the amounts adsorbed in each pore at three levels of pressure: 6×10^{-5}, 3×10^{-2} and 0.4, and these are shown in Table 1. To distinguish pores already filled, the amount adsorbed in these pores are printed bold. At the very low relative pressure of 6×10^{-5}, adsorption occurs mainly in the smallest micropores. The first three pore sub-ranges are filled completely with adsorbate while larger pores are layered with adsorbate molecules. The overall capacity calculated by our theory is 3.04 mmol/g, compared to 3.06 mmol/g calculated using the DR equation. Our approach provides a detailed distribution of this 3.04 mmol/g capacity. At a relative pressure of 3×10^{-2}, all pores having half width less than 0.588 nm are filled. This pore filling is progressed to pores of larger size when pressure increases. For example, at a reduced pressure of 0.4, the threshold pore size for complete filling is 1.266 nm, which is now in the mesopore range. Table 2 presents the results of the nitrogen adsorption onto the ACF sample at these three pressure levels calculated using the DR and our method. As seen in the table, the amount adsorbed calculated using the DR equation is by and large equal to the sum of the amounts adsorbed in all pores using our technique. The difference is more significant at the higher end of the pressure range, where adsorption in mesopores occurs in addition to that in micropores. This is because the DR equation, unable to deal with mesopores, underpredicts the data at high relative pressures, while our technique describes well the data at all pressure levels.

We now turn to the isosteric heat of adsorption, which can be calculated from the DR equation (Do, 1998) as:

$$-\Delta H = \Delta H_{vap} + E\left(\ln\frac{1}{\theta}\right)^{1/2} + \frac{E\delta T}{2}\left(\ln\frac{1}{\theta}\right)^{-1/2}$$

where δ is the coefficient of expansion of liquid adsorbate, which is very small. Figure 1 shows the plot of the isosteric heat of adsorption of nitrogen versus relative pressure at -196 °C onto the ACF sample calculated from this DR equation. To calculate the heat of adsorption from our method, we assume that the adsorption heat is approximated by the decrease in the potential energy of adsorbate, when moved from the bulk into the interior of the pore. This is shown in Table 1 for all pores. Energy released is larger in smaller pores, and proportional to the pore volume. Since the ACF sample has a distribution of pores mostly in the range from 0.32 to 0.397 nm, most of the heat comes from the pores in that range. The total heat released at any overall loading (C_μ) is obtained by summing all the individual heats released in each pore. This is the cumulative heat produced when the amount of C_μ is loaded into a clean sample. For example, from Table 1 the cumulative heat at the relative pressure of 3×10^{-2} is 55 Joule, corresponding to an amount of 6.38 mmol loaded on 1 gram of the ACF sample. The isosteric heat of adsorption

is the heat released at a given loading C_μ, i.e. it is the incremental heat produced per unit mole when the loading is incrementally increased from C_μ to $C_\mu + \Delta C_\mu$ ($\Delta C_\mu \ll C_\mu$). This is applied for nitrogen adsorption onto ACF data, and the results are shown in Figure 1. The maximum possible isosteric heat for nitrogen is ~16.2 kJ/mol if all pores having half width equal to the solid-fluid collision diameter. The isosteric heat calculated using the DR equation and our technique are quite different. The comparison between the methods and/or the justification of the suitability can be made based on the experimental measurement of the isosteric heat of the system, which is not available at this stage.

We now address the question regarding the validity of the DR equation. Figure 2 shows the isotherms of nitrogen adsorption of representative pore sub-ranges in the form of $\log(C_\mu)$ versus $\log^2(1/x)$. As seen, none of the single pore isotherms can be considered to be a straight line. However, by adding up the individual isotherms, we get the overall isotherm shown as a dotted line, which is practically a straight line, supporting the suitability of the DR equation. It is clear that the DR equation is not applicable for adsorbents having a extremely narrow pore size distribution. Samples having very skewed PSDs can not also be described by DR equation. Thus, for the DR equation to be applicable, the porous solid must have a distribution of micropores, and that distribution must not be very skewed. This explains why the DR equation is not applicable to all microporous materials.
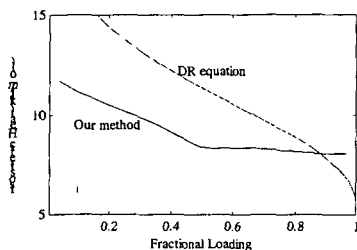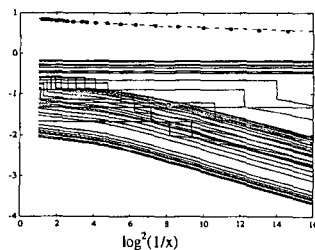

Figure 1: Plot of the isosteric heat versus loading

Figure 2: Plot of $\log(C_\mu)$ versus $\log^2(1/x)$

REFERENCES

Do, D.D., "Adsorption Analysis: Equilibria and Kinetics", Imperial College Press, London, 1998.

Dubinin, M.M., Chem. Rev., **60**, 235 (1960).

Nguyen, C. and D. D. Do, Langmuir, **15**, 3608 (1999).

Table 1: Nitrogen adsorption onto ACF at 77 K at three relative pressures (per gram of sample).

Half width	Volume	$x = 6\times10^{-5}$ loading	$x = 6\times10^{-5}$ energy	$x = 3\times10^{-2}$ loading	$x = 3\times10^{-2}$ energy	$x = 0.4$ loading	$x = 0.4$ energy
nm	cc	mmol	J	mmol	J	mmol	J
0.286	0.004	0.1256	1.32	0.1256	1.32	0.1256	1.32
0.320	0.047	1.3611	13.10	1.3611	13.10	1.3611	13.10
0.357	0.041	1.1914	10.84	1.1914	10.84	1.1914	10.84
0.397	0.029	0.2410	2.11	0.8267	7.24	0.8267	7.24
0.439	0.009	0.0367	0.31	0.2653	2.27	0.2653	2.27
0.485	0.007	0.0144	0.12	0.2069	1.74	0.2069	1.74
0.534	0.021	0.0241	0.20	0.6021	4.99	0.6021	4.99
0.588	0.030	0.0219	0.18	0.8551	7.03	0.8551	7.03
0.645	0.026	0.0136	0.11	0.3667	3.00	0.7624	6.23
0.706	0.018	0.0069	0.06	0.2249	1.83	0.5144	4.19
0.772	0.006	0.0018	0.01	0.0674	0.55	0.1688	1.37
0.843	0.005	0.0012	0.01	0.0490	0.40	0.1340	1.09
0.919	0.005	0.0010	0.01	0.0465	0.38	0.1382	1.12
1.001	0.006	0.0011	0.01	0.0516	0.42	0.1663	1.34
1.090	0.004	0.0007	-	0.0328	-	0.1141	-
1.266	0.002	0.0003	-	0.0159	-	0.0637	-
1.683	0.002	0.0002	-	0.0085	-	0.0155	-
2.249	0.002	0.0001	-	0.0066	-	0.0118	-
2.912	0.005	0.0003	-	0.0155	-	0.0278	-
3.805	0.006	0.0002	-	0.0144	-	0.0258	-
4.958	0.006	0.0002	-	0.0117	-	0.0208	-
6.444	0.009	0.0002	-	0.0134	-	0.0240	-
8.361	0.014	0.0003	-	0.0161	-	0.0288	-
9.214	0.007	0.0001	-	0.0071	-	0.0126	-
Micropore	0.254	3.042	28.39	6.240	55.09	7.318	63.87
overall	0.308	3.044		6.382		7.663	

Table 2: Nitrogen adsorption onto ACF sample calculated using our method and DR equation.

P/P_0	Overall capacity (mmol/g) Experimental	Overall capacity (mmol/g) our method	Micropore capacity (mmol/g) DR eq.	Micropore capacity (mmol/g) our method
6×10^{-5}	3.03	3.04	3.06	3.04
3×10^{-2}	6.36	6.38	6.25	6.24
0.4	7.63	7.66	6.9	7.31

CHARACTERIZATION OF ADSORPTION ON CARBON NANOTUBES USING A PULSE MASS ANALYZER

Edward W. Bittner, Milton R. Smith, and Bradley C. Bockrath
National Energy Technology Laboratory
US Department of Energy
Pittsburgh, PA 15236

KEYWORDS: Carbon nanotubes, hydrogen, adsorption of organic compounds

INTRODUCTION:
       In addition to their other special properties, carbon nanotubes also have excited considerable interest because of their potential to serve as hydrogen storage materials [1]. Several groups have reported [2-4] large values for hydrogen uptake by single walled nanotubes. Molecular simulation studies were used to identify critical structural properties that are important for development of an effective material for hydrogen storage [5]. A list of critical properties culled from the experimental and theoretical results includes the diameter of the tube, the relative number of tubes with open ends, the ease of penetration of the pore mouth to the interior of the tube, the ease of entrance into the extra-tubular space typically found between the single tube strands of rope-like structures, and the interaction potential between hydrogen and the carbon surface. In the work described below, a pulse mass analyzer similar to that originally developed to investigate the kinetics of coke deposition on cracking catalysts [6] was used to evaluate novel materials for storage potential. Direct measurements were made of weight changes in a packed bed of storage material caused by changes in the gas stream or by injection of small samples of volatile organic compounds. The amount of weight change found after injection of the samples and the "retention" time of the adsorbed material provided useful information on the characteristics of various nanotube samples. The method holds promise as an additional tool for characterization of adsorbents and storage materials.

EXPERIMENTAL:
Materials. The single wall nanotubes were obtained from Rice University (Tubes@Rice). "Fullerene Nanotubes" were used after grinding in a ball mill for ease of introduction into the sample holder, and are referred to below as raw Rice tubes. According to the analysis provided the average tube diameter is 1.36 nm. TGA analysis gave a residue weight after combustion corresponding to the expected amount of catalytic metals reported as incorporated during the synthesis. Analysis of the TGA residue by ICP led to the determination of 3.7 % nickel, 3.5 % Co, and 0.44 % Fe in the original material.
Equipment: Figure 1 is a block diagram for the apparatus including the pulse mass analyzer (PMA1500) manufactured by Rupprecht and Pataschnick. The PMA1500 is a mass measuring device that employs a tapered glass element that is stimulated to vibrate at its natural frequency. The element is made up of a long narrow hollow quartz glass tube that opens at the bottom to a 0.100 cc volume into which the sample is placed. Quartz wool and a retaining cap hold the sample in place. The element is mounted vertically in a holder in a stainless steel vessel. Carrier gas flows through the sample bed providing excellent contact. The frequency of vibration of the element is monitored via an optical system. With appropriate calibration the frequency changes are recorded as mass changes within the reactor using Equation 1. A stream of purge gas sweeps out carrier gas and other components once they have passed through the sample bed.   In addition, a valve/loop injector allows pulses of reactant gases to be introduced into the carrier gas upstream of the sample chamber. Injection of volatile organic liquids was made by syringe through a heated injection port. Mass flow controllers (Brooks, 5850E) were used to regulate the flow of both carrier and purge gases. The instrument is able to work at pressures from 1- 60 atmospheres (Brooks backpressure regulator, 5866E) and at temperatures up to 700 C.

$$\Delta m = k/ (1/f_1^2 - 1/f_2^2) \qquad (1)$$

       To determine k the instrument was equilibrated at a set temperature with no sample or sample-retaining cap and with flow rates of carrier and purge gases at nominal values. After the frequency of the vibrating element was recorded the sample-retaining cap of known mass was placed on the element and the frequency was measured a second time. Thus, k is established for the particular set of pressure, flow and temperature settings used.   The constant k has a strong temperature dependency and re-calibration must be done when the temperature is varied.
       Additional information was obtained from a quadrupole mass spectrometer (Ametek MA 100M) that sampled the exit gas stream though a   6-meter length of a capillary GC column. This detector was especially useful with the PMA in pulse mode. When a significant portion of an injection was not retained by adsorption on the sample the pulse of material passing through the bed was observed by the mass spectrometer.   Materials that were retained and then slowly

bled from the sample remained below the detection limit and were not observed. The use of a capillary column as transfer tube provided an additional means to discriminate between compounds by observing the transit time between PMA and the spectrometer. For example, the transit time for ethanol was 3.5 min. while that for 2-propanol was 5.0 min.

Gas Density Experiment

The frequency of vibration depends on the mass of the tapered element and its contents, including the weight of the gas contained within the tapered element. For example, when the carrier gas was switched from nitrogen to helium a change in mass occurred due to the change in gas density inside the element. Cycling back and forth showed reproducible gas density changes (Figure 2). Because of this, the changes in mass due simply to changes in gas density must be taken into account when the results from adsorption experiments are considered.

Adsorption Experiments

The sample bed was packed with the carbon nanotube sample and heated using helium as carrier gas and nitrogen as purge gas both at 50 cc./min. All of the experiments were performed at atmospheric pressure. Each sample was pre-treated in situ by heating to either 200 C or 700 C for 4 hours before adsorption measurements were made. Then the temperature was set for the adsorption experiment (30 C, 100 C, or 200 C) and the PMA was allowed to equilibrate for about an hour. Organic compounds (typically 1.0 or 2.0 µl as liquids), were injected into the pre-heated port (200 C) of the PMA where they vaporized rapidly in the carrier stream; the mass responses were recorded. For a carrier flow of 50 cc/min, a mass response was seen within 6 seconds, the time taken by the vaporized sample to reach the fixed bed. The mass changes were recorded as a function of time. For those compounds poorly adsorbed only a very small and transient change in mass was observed. For those strongly adsorbed, a large, rapid increase in mass was observed followed by a gradual decrease as the retained compound slowly desorbed. The gravimetric decay curve had a long tail resembling that associated with a poorly performing chromatographic column. Strongly adsorbed species took hours to desorb completely.

RESULTS:
Effect of adsorbate structure.
Hydrogen, carbon dioxide, and organic compounds were injected at 30 C, 100 C, and 200 C.

30 C. The sample holder was packed with 80.0 mg of raw Rice tubes and heated to 200 C in a stream of helium at 50.0 cc/min. with a purge gas of nitrogen at 50.0 cc/min. Following this pretreatment, the temperature of the PMA was equilibrated at 30 C for one hour. Individual pulses of hydrogen gas (3.90 mg., 1.95 mmoles) were introduced through the loop injector valve. A small peak was formed equivalent to a mass gain of 20-25 µg that returned to the baseline in a matter of seconds, indicating that only a small fraction of hydrogen injected was adsorbed then rapidly desorbed under these conditions. Pulses of CO_2 (12.8 mg., 0.291 mmoles) had a similar appearance. As typical of poorly retained compounds, hydrogen and carbon dioxide peaks appeared in the mass spectrometer following these injections and were of comparable size to those following injections into an empty reactor. Experiments conducted at a later time confirmed that little or no hydrogen adsorption occurred at 30 C by this sample, even under 27.0 atmospheres of hydrogen pressure flowing at 50 cc/min. for 3 hours. In these experiments the raw Rice tubes did not adsorb hydrogen or CO_2 to any significant extent at 30 C.

100 C. As before, pulses of hydrogen and carbon dioxide passed through the sample without significant adsorption. A series of organic compounds with similar boiling points, methanol (65.0 C), tetrahydrofuran (64.5 C), and n-hexane (68.0 C) was injected. Injections of methanol (2.0 µl.) gave reproducible changes of 1.0 mg. corresponding to 63% of the material adsorbed. A small peak for methanol was also observed by the mass spectrometer, consistent with a partially or poorly adsorbed compound. THF was adsorbed more strongly than methanol. Duplicate injections gave 86 % and 89 % of the THF retained and each injection took approximately 60 minutes to desorb. The most strongly held compound of the series was n-hexane. Of two injections, 91% and 88% were retained and it required several hours at 100 C followed by heating to 200 C to remove it completely.

200 C. At 200 C another series of compounds of disparate polarity and structure but similar boiling points was used. These were ethanol (78.5 C), 2-propanol (82.0 C), 2-butanone (79.6 C), cyclohexane (81.0 C), cyclohexene (83.0 C), and benzene (80.0 C). Figure 4 shows the PMA responses and the data are summarized in Table 1. The most striking feature of Figure 4 is the wide range of retention. Alcohols are hardly retained. For ethanol, the amount adsorbed after each 0.790 mg. (1.0 µl) injection was 0.230 mg, only 29 % of the mass injected. Desorption of the ethanol occurred within 30 seconds. About 55 % of the 2-propanol injected was retained and also desorbed rapidly. Markedly more of the cyclohexane (92 %) and cyclohexene (88 %) were

retained and each desorbed slowly. Among the three cyclic compounds, cyclohexene and benzene desorbed much more slowly than cyclohexane. The times required for the weight gain to diminish by one half (Table 1) were taken as a rough measure of relative retention.

Effect of pre-treatment temperature

After completing the adsorption experiments above, the raw Rice tubes were heated to 700 C to explore for effects due to the pretreatment temperature. This seemed appropriate because evidence has been presented [2,7] that functional groups are removed from tube openings by high temperature treatments, thus allowing for greater access to the interior of the tubes. The results show that the retention time increased significantly for some of the organic compounds compared with those found after pretreatment at 200 C (Table 1). For example, the retention time for cyclohexane doubled from 33 to 67 minutes. In general, the desorption curves for strongly retained compounds have long tails. Kinetic data from material pretreated at 200 C do not appear to obey a simple rate law. In contrast, the decay curves for all of the hydrocarbons sorbed onto nanotubes activated at 700 C were well described over the first 400 seconds by a second order rate law (eg. Figure 5). For comparison, the half lives were calculated in seconds for 1.0 mg starting weights of each as: cyclohexane (46), cyclohexene (88), benzene (89), and hexane (205). The result shows an increase in retention on introduction of one degree of unsaturation from cyclohexane to cyclohexene, but no further change on going to the aromatic compound benzene. A much greater increase was seen with n-hexane, the calculated half-life being nearly 4 ½ times that of its cyclic counterpart. This remarkable difference may be due to the ability of n-hexane to flex and bend to accommodate maximum interaction with the nanotube surface. This flexibility may allow either stronger binding to the exterior surface or alternatively, a greater tendency to be trapped within the tube. At present it seems unlikely that the desorption process can be successfully interpreted in terms of a single, well-defined adsorption site. Further studies with linear and branched hydrocarbons are needed to gain better insight into the adsorption process.

Table 1[a]
Raw Rice Tubes, Pre-treated at 200 C and 700 C

COMPOUND	BP (C)	Den. (g/ml.)	Halfwidth[b] Sec.	Halfwidth[c] Sec.
ETOH	78.5	0.789	13, 13	13
IPROH	82.0	0.780	13, 13	15, 15
CYCLOHEXANE	81.0	0.779	33, 33	67, 67
BUTANONE	79.6	0.805	40, 40	---------
CYCLOHEXENE	83.0	0.811	67, 67	133, 133
BENZENE	80.0	0.880	77, 77	107
n-HEXANE	68.0	0.659	---------	313

a) 1.0 µl injections at 200 C, helium carrier 50 cc./min. nitrogen purge 50 cc./min., duplicates shown. b) Raw Rice tubes, pretreatment 200 C. c) Raw Rice tubes, pretreatment 700 C.

CONCLUSIONS:

The interactions of hydrogen and carbon dioxide as well as several organic compounds with carbon nanotubes were investigated with a pulse mass analyzer. The pulse mass analyzer proved to be a useful tool for elucidation of structure/adsorptivity relationships in these systems. Our findings indicate that neither hydrogen nor carbon dioxide has a great affinity for these materials as compared to the organic compounds tested. Within the organic sequences, we find that alcohols are not retained as well as hydrocarbons. Moreover, unsaturation may be beneficial for adsorption in some cases (cyclohexene versus cyclohexane), but in another case (hexane) the enhanced flexibility associated with saturation of the carbon chain perhaps leads to an even greater affinity for nanotubes.

REFERENCES:
1.   M. S. Dresselhaus, K. A. Williams, P. C. Eklund, MRS Bulletin, 24, 45, (1999).
2.   A. C. Dillon, K. M. Jones, T. A. Bekkedahl, C. H. Klang, D. S. Bethune, M. J. Heben, Nature, 386,377 (1997).
3.   Y. Ye, C. C. Ahn, C. Witham, B. Fultz, J. Liu, A. G. Rinzler, D. Colbert, K. A. Smith, R. E. Smalley, App. Phys. Letts., 74, 2307 (1999).
4.   C. Liu, Y. Y. Fan, M. Liu, H. T. Cong, H. M. Cheng, M. S. Dresselhaus, Science, 286, 1127 (1999).
5.   Q. Wang, J. K. Johnson, J. Phys. Chem. B, 103,4809 (1999).
6.   F. Hershkowitz, P. D. Madiera, Ind. Eng. Chem. Res., 32, 2969 (1993).
7.   A. Kuznetsova, D. B. Mawhinney, V. Naumenko, J. T. Yates, Jr., J. Liu, R. E. Smalley, Chem. Phys. Lett., 321, 292 (2000).

DISCLAIMER:

Reference in this work to any specific commercial product is to facilitate understanding and does not necessarily imply endorsement by the United States Department of Energy.
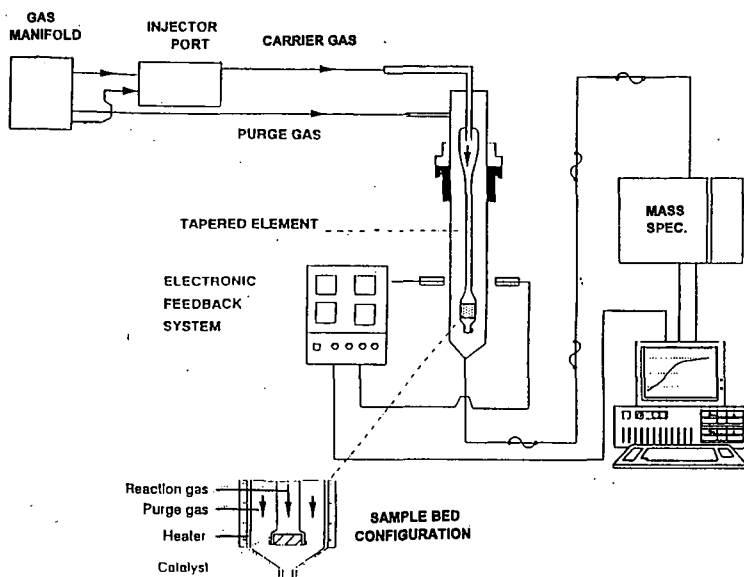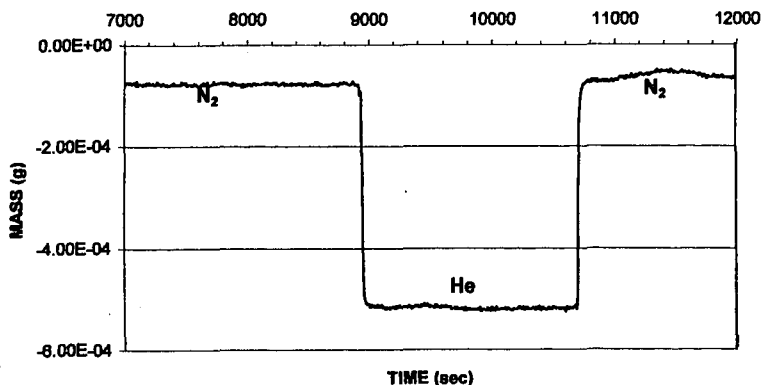

Figure 1 Block Diagram of the PMA1500

Figure 2 Gas Density Experiment, empty reactor, 30 C. carrier switch from 50cc/min N_2 to 50cc/min He to 50cc/min N_2.
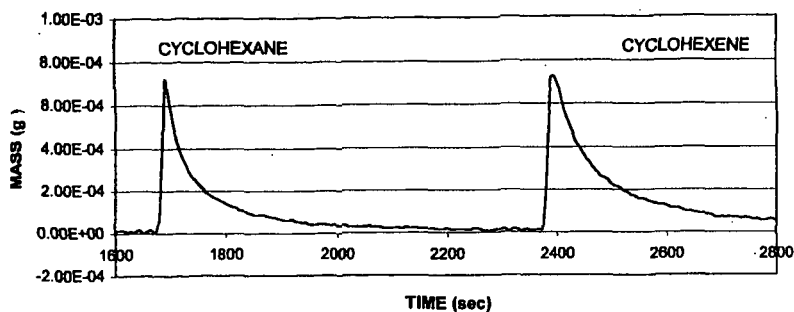
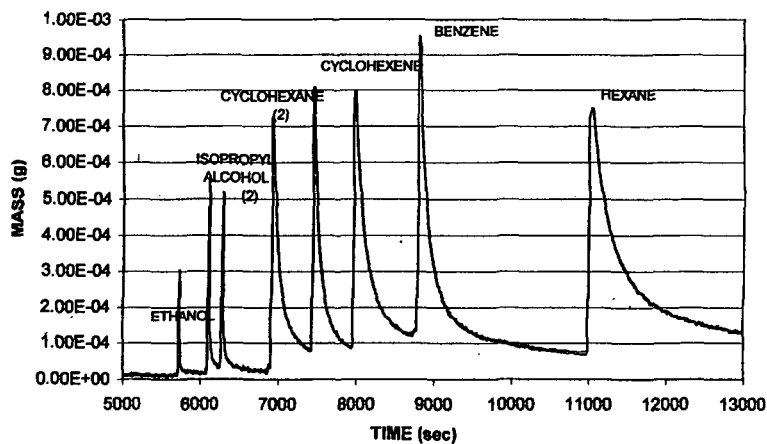Figure 3   Raw Rice tubes at 200 C, 50 cc/min He carrier with 1.0 ul. Injections of cyclohexane and cyclohexene, pretreated at 200 C

Figure 4. Raw Rice tubes at 200 C , helium carrier 50 cc./min. , pre-treatment at 700 C, 1.0 ul. injections
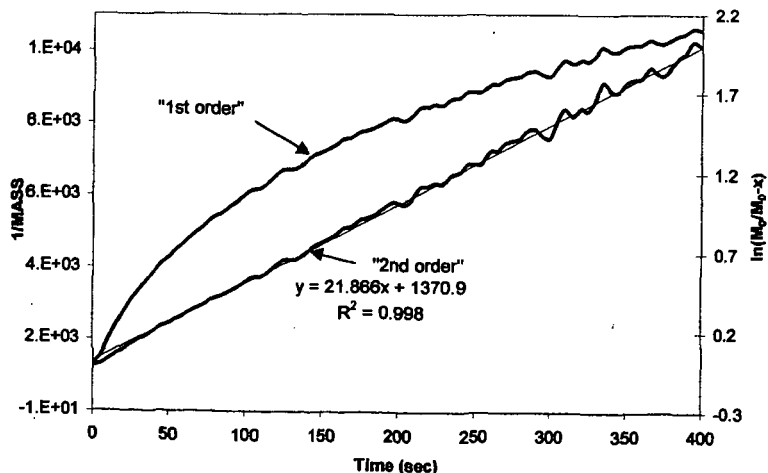
Figure 5. Rate dependence for loss of cyclohexane at 200 C (see Figure 4)

CARBON NANOTUBE ADSORBENTS

You Fa Yin, Tim Mays, Emmanuelle Alain and Brian McEnaney
Materials Research Centre, Department of Engineering and Applied Science,
University of Bath, BATH BA2 7AY, United Kingdom.

KEYWORDS: carbon nanotubes, adsorption, gas storage

INTRODUCTION

One of the more interesting applications proposed for carbon nanotubes is as storage media for fluids and solids. Of particular interest is their potential for fuel gas storage, especially hydrogen [1]. A full, experimental exploration of their potential in these fields must await developments in the production, purification and ordering of nanotubes. Meanwhile, it is possible to make some assessment of their potential as gas storage media using molecular simulations. The interior of an isolated open carbon nanotube can be viewed as a microporous or mesoporous cylindrical adsorption space (depending upon the nanotube diameter). Also, the interstices between nanotubes may provide additional adsorption space of nanometric dimensions. Therefore, we have been exploring the adsorption of gases in arrays of nanotubes using molecular simulations. In this paper we present some storage capacities for hydrogen at 298 and 77 K and nitrogen at 77 K in carbon nanotube arrays obtained from simulations and compare these to experimental measurements of adsorption in materials containing nanotubes.

MODELS AND SIMULATIONS

The model adsorption space consists of a unidirectional trigonal array of open or closed single wall carbon nanotubes, SWCNT, Figure 1. The diameter D and the nanotube separation G define the geometry of the array.
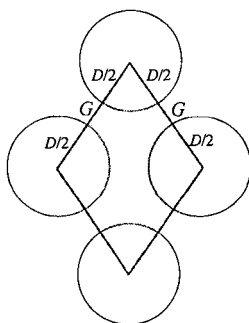

Figure 1. Model trigonal array of single-walled carbon nanotubes of diameter D and separation G. Circles are cross sections of nanotubes. The shaded area is the cross section of the simulation cell.

Table 1. Lennard-Jones potential parameters used for simulations of adsorption of H_2 and N_2 in SWCNT arrays. k_B is Boltzmann's constant.

Gas	LJ Parameter			
	σ_{ff} / Å	σ_{sf} / Å	(ε_{ff} / k_B) / K	(ε_{sf} / k_B) / K
Hydrogen	2.96	3.19	41.5	35.4
Nitrogen	3.572	3.494	93.98	53.52

We have also studied square arrays of SWCNT [2]. The Grand Canonical Monte Carlo Ensemble method [e.g., 3] was used to simulate equilibrium adsorption of gases in the model array. A single site Lennard-Jones (LJ) 12:6 pair potential was used to represent interactions between gas molecules. The interaction between an adsorbate molecule and a single nanotube was obtained by integration of the LJ potential over the nanotube surface; this potential is applicable to adsorption inside and outside tubes (endohedral and exohedral adsorption [4]). The LJ length (σ) and energy (ε) parameters for fluid-fluid (ff) and solid-fluid (sf) potentials are listed in Table 1. The cross section through the simulation cell, perpendicular to the length of the nanotubes, is a parallelogram, Figure 1. The length of the cell parallel to the nanotubes was

normally $10\sigma_{ff}$, although this could be extended to increase the number of molecules in the cell and so reduce errors. The Peng-Robinson equation of state was used to calculate the chemical potentials of bulk gases [5]. The main output from the simulations was the average number of molecules adsorbed in the simulation cell as a function of pressure.

RESULTS AND DISCUSSION

Hydrogen Storage at 298 K and 77 K.   The amount of usable gas in a gas storage system is the delivered capacity, *i.e.*, the amount of gas stored at the higher (storage) pressure less the amount retained in the container at the lower (delivery) pressure. The delivered capacity can be expressed on a gravimetric or volumetric basis; here, a gravimetric basis is considered. For hydrogen, storage and delivery pressures were normally 70 and 1 bar respectively. For studies of the effects of storage pressure on the hydrogen capacity, the storage pressure was varied from 1 to 200 bar. The US DOE hydrogen plan for a fuel cell powered vehicle requires the storage system to have a delivered gravimetric capacity of 6.5 wt% H_2 [1].
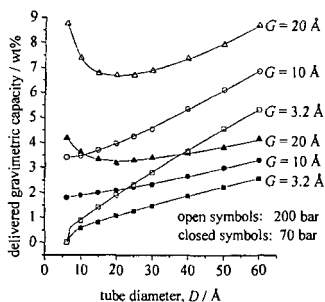

Figure 2. Delivered gravimetric hydrogen capacity at 298 K as a function of tube diameter in trigonal arrays of open single-walled carbon nanotubes with different separations G, for storage pressures of 70 and 200 bar.

Figure 2 shows the delivered gravimetric capacities of trigonal arrays of open SWCNT at 298 K and at storage pressures of 70 and 200 bar. For most of the arrays, capacity increases with increasing nanotube diameter, D, and tube separation, G. The effect of tube diameter on capacity is as expected while the effect of tube separation shows that exohedral adsorption in the interstices between the nanotubes is important. Significant amounts of hydrogen can be stored in the arrays, but none of them achieves the DOE target capacity at 298 K and a storage pressure of 70 bar. The DOE target capacity is achieved at 298 K and 200 bar storage pressure for SWCNT with a wide range of diameters in arrays with a spacing of 20 Å.
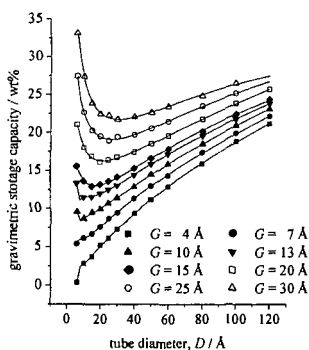

Figure 3. Gravimetric hydrogen storage capacity for trigonal arrays of open single-walled carbon nanotubes at 77 K and 70 bar as a function of tube diameter D and separation G.

The effects of increases in D and G on storage hydrogen capacities at 77 K and 70 bar, Figure 3, are broadly similar to those found at 298 K. The DOE target capacity is reached for arrays with a wide range of D and G values. For arrays with a spacing of 30 Å, the DOE target is exceeded by a considerable margin. The maximum delivered hydrogen capacity of ~33 wt% is reached with an array consisting of widely spaced narrow nanotubes ($D = 6$ Å, $G = 30$ Å) where exohedral adsorption dominates. The non-linear variations in capacity for arrays with $D < 30$ Å and $G > 7$ Å, Figure 3, are the result of complex geometrical factors affecting the space available for adsorption in the simulation cell. The volume of the simulation cell is proportional to $(D + G)^2$, while the mass of carbon in the cell is proportional to D. Thus, when $G \ll D$, the volume available per unit mass is $\sim D$, i.e., the capacities increase with D nearly linearly as in Figure 3. When $G \gg D$, the volume available per unit mass is $\sim 1/D$, i.e., the capacities decrease with increasing D.

Nitrogen Adsorption at 77 K. Figure 4 shows the gravimetric saturation capacity for nitrogen at 77 K and relative pressure $P/P_0 = 1$ for trigonal arrays of open SWCNT as a function of D and G. Qualitatively, the effects of increases in D and G on capacity are broadly similar to those found for hydrogen at 77 K, Figure 3. However, the gravimetric capacities for nitrogen at $P/P_0 = 1$ are more than 10 times higher than that for hydrogen at 70 bar in arrays of the same geometry. This is because (1) the critical temperature for nitrogen is much higher than for hydrogen, and (2) the molecular mass of nitrogen is 14 times that of hydrogen.
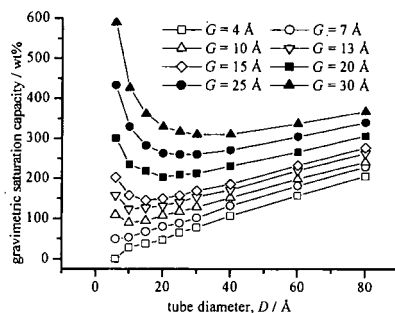

Figure 4. Gravimetric nitrogen saturation capacity for trigonal arrays of open single-walled carbon nanotubes at 77 K and relative pressure $P/P_0 = 1$ as a function of tube diameter D and separation G.

Comparisons of simulations with experiment.   In the case of nanotubes, comparisons between experimental and simulated gravimetric adsorption capacities are complicated because experimental amounts adsorbed have been measured on nanotube samples that have different purities and that have not been ordered into arrays. Also, as the foregoing shows, simulated gravimetric capacities depend upon the geometry of the array.

Comparison of hydrogen capacities at 298 and 77 K.

Table 2. Comparisons of gravimetric hydrogen storage capacities from experiments and molecular simulations.

System	T / K	P / bar	H$_2$ capacity / wt%	Ref
SWCNT, 50% purity (E)	300	101	4.2	[6]
Trigonal array of open SWCNT (S)	298	100	4.7 max [a]	d
SWCNT, high purity (E)	80	72	8.25	[7]
Trigonal array of open SWCNT (S)	77	70	0-33 [b]	d

(E) – Experiment; (S) Simulation. a. $D = 60$ Å, $G = 10$ Å; b. $D = 6$ Å, $G = 30$ Å. d. this work

An experimental measurement of hydrogen capacity for 50% pure SWCNT at ambient temperatures and ~101 bar of 4.2 wt% [6], see Table 2, is in reasonable agreement with the hydrogen capacity at similar temperatures and pressures (4.7 wt%) obtained from simulations for trigonal arrays of open SWCNT with $D = 60$ Å, $G = 10$ Å. Molecular simulations of hydrogen storage at 77 K and 70 bar on trigonal arrays of open SWCNT with $D = 7$ Å, $G = 30$ Å, produce a

very high capacity (33 wt%, Table 2). This may be compared with an experimental measurement made on high purity SWCNT at similar temperatures and pressures [7] (8.25 wt%, Table 2). This simple comparison suggests that the experimental hydrogen capacities of nanotubes at 77 K can be increased substantially by developing ordered arrays.

Comparison of nitrogen capacities at 77 K. Some experimental measurements of adsorption of nitrogen on SWCNT have been reported by Alain *et al.* [8]. Here, a more precise comparison between simulation and experiment can be made because the dimensions of the nanotubes ($D \sim$ 13.8 Å) are known from high-resolution transmission electron microscopy images. HRTEM also showed that the SWCNT were present in closed packed bundles with $G \sim 3.2$ Å. A comparison of the isotherm for these nanotubes measured using a volumetric apparatus with the results from simulations in trigonal arrays of open and closed SWCNT ($D = 13.8$ Å, $G = 3.2$ Å) is in Figure 5.
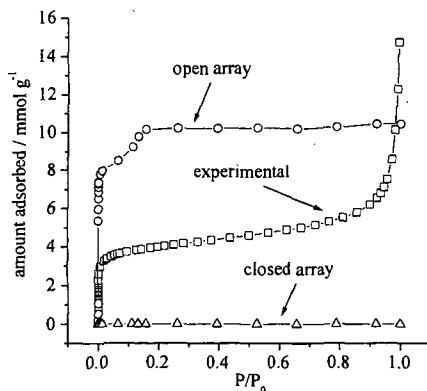

Figure 5. Comparison of experimental isotherms of nitrogen adsorbed at 77 K in single-walled carbon nanotubes to simulated isotherms for the same array geometry ($D = 13.8$ Å, $G = 3.2$ Å) with both open and closed nanotubes.

The simulations show that there is no adsorption in the array of closed SWCNT because the interstitial space is too small to admit nitrogen molecules. The simulated isotherm for the array of open SWCNT is close to Type 1 in the BDDT classification, indicating, as expected, that the nanotubes are behaving as microporous adsorbents. In the case of the experimental isotherm the steep rise at low relative pressures also indicates the presence of micropores. From the average bundle size and tube diameter [8], it is estimated that an average bundle contains about 50 nanotubes. Therefore, the specific surface area of the bundles is ~ 235 m^2 g^{-1}. The measured BET surface area of the nanotube sample is 302 m^2 g^{-1} [8], larger than the estimated bundle surface area. It is believed that the majority of the SWCNT are closed, but it is possible that a small proportion are open so that they may make a contribution to the adsorption at low relative pressures. In addition, the impurities in the sample may also contribute to the BET surface area. The steep rise in adsorption at high relative pressures probably reflects condensation in the sample, possibly between the nanotube bundles. We are carrying out further simulations and experimental measurements of adsorption in carbon nanotubes to clarify these points.

CONCLUSIONS

Molecular simulations of adsorption of hydrogen at 298 K and 70 bar in ordered arrays of SWCNT show that significant storage occurs. However, this is ~70% of the DOE target capacity of 6.5 wt%. Experimental measurements of gravimetric hydrogen capacity at ambient temperatures and ~100 bar for carbon nanotube samples are similar to those predicted from simulations. The simulations also show that the target gravimetric hydrogen capacity can be achieved with ordered arrays of nanotubes at 77 K and 70 bar with a wide range of diameters and spacings. Experimental measurements of hydrogen capacity under similar conditions lie within the range predicted from simulations, but at ~25% of the predicted maximum capacity. Simulated and experimental measurements of nitrogen adsorption at 77 K on SWCNT both show some evidence for microporous adsorption. Also, the experimental isotherms show evidence for

capillary condensation at high relative pressures, possibly occurring between bundles of nanotubes.

ACKNOWLEDGEMENTS

REFERENCES

1. Dillon, A. C., Jones, K. M., Bekkedahl, T. A., Kiang, C. H., Bethune, D. S. and Heben, M. J. (1997). Storage of hydrogen in single-walled carbon nanotubes. *Nature* **386**(6623), 377-379.

2. Yin, Y.F., Mays, T. J. and McEnaney, B. (1999). Adsorption of nitrogen in carbon nanotube arrays. *Langmuir* **15**, 8714-8718.

3. Allen, M. P. and Tildesley, D. J. (1987). Computer Simulation of Liquids. Clarendon Press, Oxford, p.127.

4. Yin, Y. F. and Mays, T. J. (1998).   Adsorption in carbon nanotubes. *Carbon '98*, Strasbourg, France, 831-832.

5. Peng, D.Y. and Robinson, D.B. (1976). A new two-constant equation of state. *Ind. Eng. Chem. Fundam.* **15**, 59-64.

6. Liu, C., Fan, Y. Y., Liu, M., Cong, H. T., Cheng, H. M. and Dresselhaus, M. S. (1999). Hydrogen storage in single-walled carbon nanotubes at room temperature. *Science* **286**, 1127-1129.

7. Ye, Y., Ahn, C. C., Witham, C., Fultz, B., Liu, J., Rinzler, A. G., Colbert, D., Smith, K. A. and Smalley, R. E. (1999). Hydrogen adsorption and cohesive energy of single-walled carbon nanotubes. *Applied Physics Letters* **74**(16), 2307-2309.

8. Alain, E., Yin, Y. F., Mays, T. J. and McEnaney, B. (2000). Molecular simulation and measurement of adsorption in porous carbon nanotubes. *Stud. Surf. Sci. Catal.* **128**, 313-322.

POROSITY OF CARBON NANOTUBES

Marit Jagtoyen, James Pardue, Terry Rantell, Eric Grulke and Frank Derbyshire

University of Kentucky, Center for Applied Energy Research
2540 Research Park Drive, Lexington, KY 40511, USA
E-mail: jagtoyen@caer.uky.edu

Progress in the large-scale production of carbon nanotubes has opened up possibilities for new applications in some areas of adsorption and catalysis. In this paper we will discuss the characterization of single and multiwalled nanotubes by nitrogen, butane and methane adsorption. Nitrogen adsorption data will be used to calculate pore size distributions of the nanotubes. The incorporation of carbon nanotubes into pitch to change the porosity of the resultant activated carbon will also be discussed. By altering the pore structure of the pitch-based carbon fibers from highly microporous to a wider size distribution of micro and mesopores, new applications of the fibers can be envisaged in areas of environmental science and catalysis.

INTRODUCTION

Recently, methods have been developed at the University of Kentucky to synthesize high purity multiwalled carbon nanotubes (MWNT) in quantities that allow the study of the bulk properties of the material. Continuing work is aimed at improving both the rate of production, by operating on a larger scale, and a simplified process to reduce costs. The suitability of use of nanotubes in applications of gas adsorption, separation and catalysis has been investigated. Currently there is little reliable information available in the literature concerning the pore structure and surface properties of pure carbon MWNTs. Most work have been conducted on samples of low or uncertain purity that may contain high concentrations of amorphous and/or graphitic carbon as a contaminant. In contrast, materials produced at the Center for Applied Energy Research (CAER) are typically better than 95% pure MWNT.

The core diameter of single wall nanotubes (SWNT) is close to 1 nm, with little variation between samples, a value which falls in the range normally defined by micropores (pore entrance diameter < 2nm). MWNT, in contrast, show a small variation in core diameter, typically ranging from 3.5 to 7nm, and hence fall in the mesopore range (diameters 2 to 50nm). The uniformity of the nanotubes and thus the narrow distribution of pore sizes present in the sample, should make them excellent materials for gas separation applications. As an example, the diffusion rate of methane into MWNT bundles has been found to be up to ten times faster than that for butane, offering the prospect for the development of systems providing efficient molecular sieves.

Another objective of the current work is to use carbon nanotubes to modify the porosity of pitch-based activated carbon fibers (ACFs). These are normally derived from isotropic petroleum pitch precursors through a sequence of well-defined process stages, culminating in activation of the isotropic carbon fibers in steam or nitrogen, generating the high surface area and pore structure that is typified by a narrow distribution of micropores. The objective of dispersing mesoporous carbon nanotubes in the isotropic pitch before processing into activated carbon fibers is to produce fibers that are not only significantly more mesoporous, but also show significant improvements in other properties, e.g. strength and electrical conductivity. This could enable the procurement of activated carbon fibers with pore structures tailored to specific environmental applications. This paper will focus on the porosity characterization of multiwalled nanotubes and comparison with single walled tubes, and the introduction of these tubes into pitches to alter the pore structure of the product activated carbon.

EXPERIMENTAL

Single wall nanotubes (SWNTs) manufactured by Carbolex Inc. using a carbon arc process with Ni/Y catalyst, were purified by refluxing in 2M nitric acid for 24 hours, filtered and then sonicated in dimethyl sulphoxide (DMSO) for 12 hours before drying. Multiwalled carbon nanotubes were produced at CAER by the catalytic decomposition of a ferrocene-xylene mixture at a temperature of about 700°C and at atmospheric pressure (1). Scanning electron microscopy (SEM) was used to estimate the purity of the MWNT samples. One of the MWNT samples was leached in hydrochloric acid to reduce the amount of iron catalyst from an as-produced concentration of about 5%, in order to determine its affect upon pore structure and accessibility. In a parallel series of experiments, the effect of the inclusion of carbon nanotubes in a pitch matrix precursor on the porosity of the active carbon derived from it was determined. A sample

of SWNT suspended in DMSO was dispersed in the pitch by intimately mixing the suspension with a solution of the pitch in a suitable solvent. A high power ultrasonic probe was used to ensure that the nanotubes were completely dispersed before the solvents were recovered by distillation. The pitch samples were then activated by heating in a steam atmosphere at 877°C to generate an active carbon. Characterization of the pore structures was carried out using an OMNISORB 610 instrument to obtain nitrogen adsorption isotherms at 77 K. The mesopore volume, surface area and pore size distribution were calculated using the BJH method (2).

RESULTS

Porosity of Nanotubes

Adsorption isotherms of SWNT and MWNT are compared in Fig. 1. The MWNT sample is ~100% purity as determined by SEM. The adsorption isotherms for both samples are typical of mesoporous carbons, with the MWNT giving considerably higher nitrogen adsorption. The mesopore size distribution of the two samples is shown in Figure 2. The multiwalled sample clearly has a higher mesopore volume with an average pore size of ~3.5 nm. This corresponds approximately to the diameter of the central core of the MWNTs as determined by transmission electron microscopy to be in the range of 3-7 nm, Figure 3. Elsewhere, it has been shown that the average pore diameter of MWNTs is 4-6 nm (3). The calculated mesopore volumes of MWNTs and SWNTs are shown in Table 1. The SWNT have a mesopore volume of 0.05 cc/g while that of the pure MWNT sample is about 0.45 cc/g.

Table 1. Mesopore volume of different nanotube samples.

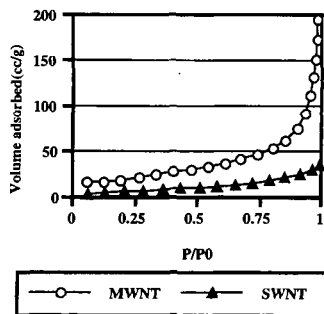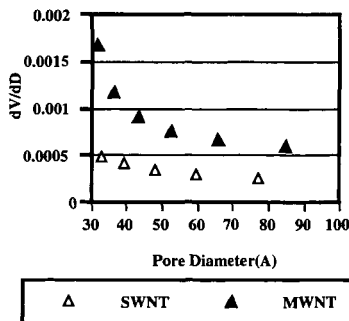| Sample ID	Purity (% MWNTs)	Mesopore volume(cc/g)
SWNT	~100%	0.05
MWNT-A	~95%	0.47
MWNT-B	~100%, leached	0.48

Figure 1. N₂ Adsorption isotherm of MWNT and SWNT

Figure 2. Pore size distribution of SWNT and MWNT

909

Observations by TEM have shown that small iron particles are present at the ends of the tubes, a consequence of their catalyzing nanotube growth. They are also found intermittently along the core of the innermost tube and in this location may not be accessible by the hydrochloric leaching agent. The acid treatment removes approximately 50% of the iron catalyst and probably improves access to the core of the MWNTs by removing iron from the ends. Even though the total mesopore volume is not significantly enhanced, Table 1, it does seem to broaden the mesopore size distribution slightly.
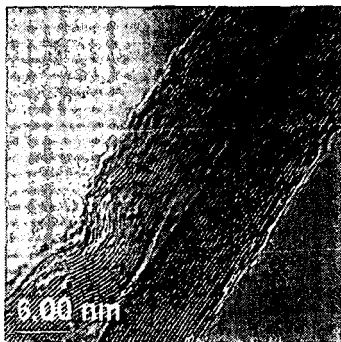
Figure 3. TEM micrograph of MWNT

Addition of SWNTs to pitch to modify the pore structure of activated carbons

A nitrogen adsorption isotherm of activated carbon derived from pitch powder is shown in Figure 4 together with that of the pitch with 5% SWNT incorporated. The pure petroleum pitch based carbon has a very microporous structure, illustrated by the flat isotherm, whereas the pitch with SWNT incorporated has a mesoporous structure, shown by the higher adsorption of nitrogen at high partial pressure. This isotherm is typical of a mesoporous activated carbon. The inclusion of SWNT in the precursor pitch has generated a high mesopore volume in the product active carbon without impairing the retained microporosity. The pore size distribution of the pitch with and without nanotubes is shown in Figure 5. It is evident that the activated carbon has a very narrow pore structure while the carbon with SWNT has a broader pore structure with more porosity in the mesopore range (20-500A).
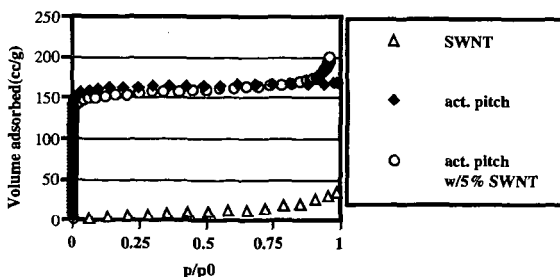

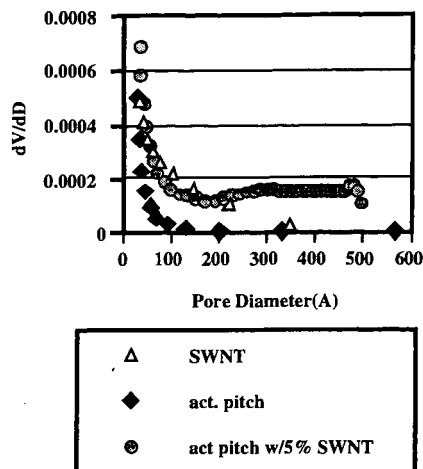**Figure 4. N$_2$ adsorption isotherms of activated pitch and activated pitch with SWNT**

Figure 5. Pore size distribution of activated pitch and activated pitch with SWNT

ACKNOWLEDGEMENTS

REFERENCES

1. Andrews, R., Jacques, D., Rao, A. M., Derbyshire, F., Qian, D., Fan, X., Dickey, E.C., Chen, J., Chem Phys Lets, 1999, April 16.
2. Gregg, S.J, Sing, K.S.W, in *"Adsorption,Surface Area and Porosity"*, 2nd ed., Academic, London , 1982, 94-100.
3. Bonnamy, S., Gaucher, H., Metenier K., Pellenq, R., Nalimova V., Frackowiack, E.. and Beguin, F., Abstract presented at the British Carbon Group, Leeds, 1998.